IPNO DRE 93-32

EXCLUSIVE AND RESTRICTED INCLUSIVE REACTIONS INVOLVING THE ^{11}Be ONE-NEUTRON HALO

R. Anne, R. Bimbot, S. Dogny, H. Emling, D. Guillemaud-Mueller, P.G. Hansen, P. Hornshøj, F. Humbert, B. Jonson, M. Keim, M. Lewitowicz, P. Møller, A.C. Mueller, R. Neugart, T. Nilsson, G. Nyman, F. Pougheon, K. Riisager, M.G. Saint-Laurent, G. Schrieder, O. Sorlin, O. Tengblad and K. Wilhelmsen Rolander.

Exclusive and Restricted Inclusive Reactions Involving the ^{11}Be One-Neutron Halo

R. Anne[1)], R. Bimbot[2)], S. Dogny[2)], H. Emling[3)], D. Guillemaud-Mueller[2)], P.G. Hansen[4)], P. Hornshøj[4)], F. Humbert[5,a)], B. Jonson[6)], M. Keim[7,a)], M. Lewitowicz[1)], P. Møller[4)], A.C. Mueller[2)], R. Neugart[7,a)], T. Nilsson[6)], G. Nyman[6)], F. Pougheon[2)], K. Riisager[4)], M.-G. Saint-Laurent[1)], G. Schrieder[5,a)], O. Sorlin[2)], O. Tengblad[8)] and K. Wilhelmsen Rolander[6)]

1) *GANIL, F-14 021 Caen Cedex.*

2) *Institut de Physique Nucléaire, IN2P3-CNRS, F-91 406 Orsay Cedex.*

3) *GSI, Postfach 11 05 52, D-64220 Darmstadt.*

4) *Institut for Fysik og Astronomi, Aarhus Universitet, DK-8000 Aarhus C.*

5) *Institut für Kernphysik, Technische Hochschule, D-64289 Darmstadt.*

6) *Fysiska Institutionen, Chalmers Tekniska Högskola, S-412 96 Göteborg.*

7) *Institut für Physik, Universität Mainz, D-55099 Mainz.*

8) *PPE Division, CERN, CH-1211 Genève 23.*

Received:

---

[a] Supported by Bundesministerium für Forschung und Technologie under contract numbers 06DA 641I and 06MZ 188I.

Abstract: Reactions of a 41 MeV/u beam of the radioactive halo nucleus ^{11}Be have been studied with a counter telescope coupled to an array of neutron detectors covering angles to 97^0. The technique allows to determine single-neutron inclusive and exclusive angular distributions. The targets (Be, Ti and Au) were chosen to illustrate the relative roles played by nuclear and Coulomb mechanisms. The channels leading to ^{10}Be, the dissociation channels, correspond to impact parameters larger than the sum of the radii of the target and the ^{10}Be core. It is shown that for the dissociation process it is possible to account almost quantitatively for the integral, single- and double-differential cross-sections from models without free parameters including the Coulomb, Serber and Glauber (diffraction dissociation) mechanisms. The neutron distributions from the non-dissociative reaction channels show little individuality and it is convenient to group them together as the channel "neutron plus anything different from ^{10}Be". We refer to these as "restricted inclusive" reactions. These seem to be a promising tool for obtaining accurate information on the halo wave function in momentum coordinates.

Key Words: NUCLEAR REACTIONS Be, Ti, Au (^{11}Be, n+^{10}Be+X), E=41 MeV/nucleon, measured inclusive and exclusive $\sigma_n(\vartheta)$ to 97^0, double-differential $\sigma(\vartheta,E_n)$ near 0^0, and integral $\sigma(^{10}Be)$. Analysis in terms of Coulomb, Serber and diffractive mechanisms.

1. Introduction

The nuclei with a neutron halo, see e.g. the reviews [1-8], pose a peculiar experimental problem. Having in most cases only one bound state in addition to an almost structureless continuum, these nuclei are not amenable to the usual spectroscopic methods of nuclear structure physics. The attention has instead focused on nuclear reactions. Among those, the study of momentum distributions [9-11] from the fragmentation of halo nuclei has turned out to be especially fruitful. At first it was hoped that the measured momenta under favourable circumstances would be representative of those of the halo ground state, in other words that the experiments in this limit in the spirit of the Hüfner-Nemes model [12] of fragmentation would determine (the square of) the Fourier transform of the ground-state wave function. We know now that although this is often approximately true, there are unavoidable modifications caused by the reaction mechanisms, and these become a major problem when it comes to studying the finer points such as the expected existence of neutron-neutron correlations [6,13] in nuclei with a two-neutron halo such as ^{11}Li. Barranco et al. [14] have recently made an attempt at interpreting the neutron distributions from the dissociation of this nucleus in an approach including all reaction mechanisms. They suggest that the results for different targets represent a variation of mixtures of four basic and quite different distributions that somehow conspire to give the observed [10,15], narrow angular distributions, which are almost identical for light and heavy targets.

In order to clarify the interplay between structure and reaction mechanism, the present work has investigated fragmentation reactions of ^{11}Be, so far the only known case of a one-neutron halo. Its structure is, if not completely simple, then at least sufficiently transparent to allow a quantitative interpretation. The strategy is the same as in our previous experiments [10,15] on ^{11}Li, namely to measure the angular distributions of the fast forward neutrons. Since these are the constituents of the halo they are clearly the fragments most suited for conveying information about its structure. The approach is again rigorously quantitative. Unlike a good fraction of other published results in this sub-field, the measured cross-sections reported in the following are on an absolute scale. We compare them with simple but quantitative estimates, usually with no free parameters. Nevertheless, the agreement is in most cases very good, which we take as a sign that the main features of the observed phenomena are correctly understood.

The background for the present paper would not be complete without mention of the deuteron, the mother of all halo nuclei and certainly the only one with both a proton and a neutron halo. The *rms* neutron-proton distance in the deuteron is 4.2 fm [16] as compared with a calculated [17] value for the ^{10}Be-neutron distance of 6.5 fm corresponding to a super-deuteron. The reaction mechanisms that will be discussed

in the following were all developed for the deuteron; Coulomb dissociation by Oppenheimer [18] and Dancoff [19], stripping by Serber [20], and diffraction dissociation by Glauber [21]. The blend of these has later been refined by many others, in particular by Fäldt [22].

The structure of the paper is simple. After a description of the experimental techniques in Section 2 follows in Section 3 a survey of previous experiments and calculations on ^{11}Be and of the main theoretical concepts used in our calculations. The experimental results follow in Section 4. Our preliminary paper [23] showed data out to 30^0 laboratory angle and compared these with separate calculations for Coulomb and nuclear processes. The final results appearing here have data out to 97^0, and they are compared with a unified theory comprising all three mechanisms and giving total as well as differential cross-sections. We also present the energy spectra of the neutrons near 0^0. Finally, the neutron angular distributions recorded in anti-coincidence with a fast ^{10}Be nucleus are investigated. These distributions seem to hold some promise for a more direct approach to the true halo wave function.

2. Experimental Techniques

The main aim of the experiments was to measure energy spectra and angular distributions of the forward fast neutrons from reactions of ^{11}Be. Three targets were used, beryllium (Z=4), titanium (Z=22), and gold (Z=79). These were chosen in order to illuminate the relative contributions of nuclear and Coulomb interactions, dominant for beryllium and for gold, respectively. An essential part of our experimental strategy was that the fast charged fragments from the reactions were recorded in a counter telescope and in coincidence with the neutrons so that the information could be sorted according to different reaction channels. Since the ^{10}Be core has little chance of remaining intact after a collision with the target nucleus, the channel with this nucleus as a fast outgoing fragment must predominantly represent collisions that take place for impact parameters larger than the sum of the core and target radii. These reactions leading to ^{10}Be we refer to as dissociation reactions. They are very sensitive to the halo structure.

The single-neutron inclusive angular distributions, which have important contributions from core-target collisions, were presented and briefly commented on in our previous paper [23]. In the present paper we have found it more instructive to present the data with the dissociation reactions removed. The result of this is what we call "restricted inclusive" distributions corresponding to the channel "neutron plus anything except ^{10}Be". The anti-coincidence requirement is possible because the particle telescope was placed to give 100% coverage of the outgoing fragments. The events thus selected are predominantly those for which the impact parameters are smaller than the sum of the core and

target radii. Exclusive sub-sets of the same class of events could be selected by choosing a particular outgoing fragment such as a lithium or helium nucleus.

From the telescope data alone information was obtained on the integral dissociation cross sections and on cross-sections for the formation of other charged fragments such as boron isotopes.

The following is a survey of the techniques used in the experiment and analysis. Much additional information, both on techniques and on the physics results from the analysis, can be found in two Ph.D. theses based on this work, one by Dogny [24] and one by Wilhelmsen Rolander [25].

2.1 THE RADIOACTIVE BEAM

A secondary beam of ^{11}Be was produced by bombardment of a 540 mg/cm^2 beryllium target with 63 MeV/u fully stripped ^{18}O ions from the GANIL coupled cyclotron facility. The fragmentation products were subsequently sifted in the LISE3 spectrometer [26], in which the purification proceeds in three stages. There is first a selection in magnetic rigidity, secondly a selection based on the energy loss in a wedge-shaped degrader and effected by a second magnetic analysis, and, finally, a third selection in velocity with a Wien filter with crossed electric and magnetic fields.

With a momentum acceptance of LISE3 limited by slits to 0.5%, with a thickness in the middle of 485 mg/cm^2 of the "achromatic" aluminium degrader and with a dispersion of the Wien filter of 1.1 mm for 1% of velocity increment, the purity of the ^{11}Be beam was better than 10^{-4}. As a result of the reduced momentum acceptance, the count rate of 1500 atoms/s gave an acceptable level of pile-up and at the same time matched the capacity of the data acquisition system.

The incoming fragments were identified on an event-by-event basis through their time of flight between the detector ΔE_1 (see the inset in Fig. 1) and a thin plastic scintillator placed 25 m upstream in the achromatic focal point at the exit of the second magnetic analyzer. The average energy of the incident beam was 45.2 MeV/u before and 44.1 MeV/u after ΔE_1.

2.2 DETECTION OF THE REACTION PRODUCTS

The experimental arrangement is shown in Fig. 1. The reaction chamber under vacuum contained the target and telescope unit indicated in the inset, which shows the target sandwiched between two 300 μm silicon detectors and followed by a 5500 μm silicon detector E_3, which measured the energy of the charged fragment. A thick cylindrical copper

collimator (not shown) in front of the sandwich excluded reactions in the detector holders.

The three targets were matched in thickness to 370, 454 and 724 mg/cm^2 for Be, Ti and Au, respectively, in order to have approximately the same energy loss for the incident beam, leading to calculated [27] exit energies of 37.7 (Be), 37.5 (Ti), and 36.9 (Au) MeV/u. The targets were mounted on a wheel, which also contained an empty frame for the background measurement, which was made with the beam energy after ΔE_1 reduced to 37.4 MeV. This allows to correct for reactions occurring in the thick silicon detector.

In order to minimize the loss of neutrons, the scattering chamber was equipped with a thin (0.5 mm) exit window of stainless steel. An array of 32 neutron detectors (Fig. 1) of varying sizes surrounded the target at a distance of 3 m. The neutron energy was determined from the time of flight relative to the ΔE_1 detector, and gamma rays and neutrons were distinguished by pulse-shape discrimination. The pulse-height discriminator threshold was set at 1 MeV measured by the Compton edge of the ^{60}Co gamma ray and corresponding to 3 MeV energy of the recoil proton, a setting that strongly influences both the detector efficiency and the probability of cross talk between the detectors.

The absolute efficiencies were calculated for the 15 cm thick detectors by a Monte Carlo technique [28] and varied from 34% at 25 MeV to 20% at 70 MeV. These results were scaled to the detectors of other thicknesses. Measurements with 14 MeV neutrons [29] demonstrated that contributions from cross talk were negligible, also for the central array.

2.3 DATA TAKING AND ANALYSIS

The trigger for the data recording was the arrival of a fragment of interest in the first detector of the telescope. Since the number of neutrons per trigger was only 0.4%, it was advantageous to use neutron and gamma events in the neutron detector array as a subsidiary trigger according to which the output of the ADCs and TDCs were stored on tape either as "short events" containing only heavy-ion parameters or as "long events" containing data from the neutron detectors.

The analysis of the telescope data proceeded via the selection of a ^{11}Be event from the energy deposited in ΔE_1 and from the time of flight of the ion. From these, a spectrum as a function of the ion energy E_3 was created for each target and a background spectrum (measured with the empty target frame) and similarly treated was normalized to the number of incoming ^{11}Be and subtracted. In this representation a clear ^{10}Be peak emerged which allowed the determination of the dissociation cross-

section. The selection is illustrated in Fig. 2, which shows data with the additional requirement of a neutron coincidence, see below.

Cross-sections for the fragmentation channels, leading to the formation of helium, lithium, boron, and lighter beryllium isotopes, could be obtained from the two-dimensional plot of ΔE_2 *versus* E_3, which provides particle identification. It is interesting to note that we also observed fast boron ions corresponding to the net pick-up of one proton by the beryllium core, see Fig.3. The most striking result is probably the formation of ^{12}B with a cross-section of 5 mb. It is, of course, likely that this is produced in a multi-nucleon exchange reaction.

The double-differential neutron distributions were obtained for each detector by selecting the neutron events on the basis of the pulse-shape discrimination signals. For the central array, the gamma background, which is largely isotropic, was so small that the gamma and neutron groups could not be distinguished, and there all events were included. The neutron-gamma identification is, anyway, of little importance except for the largest angles because the reaction gamma rays to a very good approximation are eliminated by their flight time alone. In order to obtain the single-neutron exclusive and restricted-inclusive events the data were further sorted according to the telescope signals by setting an appropriate window as an area in the two-dimensional particle-identification spectrum ΔE_2-E_3. The neutron spectrum could then be obtained from the time-of-flight data. The background spectrum of neutrons arising from reactions in the silicon counters was determined in the same way from the run with the empty target and was normalized to the same number of ^{11}Be ions in ΔE_1 and subtracted.

The true neutron intensity normalized to the number of incoming ^{11}Be projectiles could now be obtained by dividing out the solid angle subtended by the detector and the energy-dependent detection efficiency. Fig. 2 shows the telescope data with the additional demand of a neutron coincidence. It demonstrates that the gold target predominantly leads to the formation of ^{10}Be, while the lighter targets have an important component at lower energies which must come from reactions of the ^{10}Be core with the target. The figure is also an illustration of the Achilles' heel of our experimental method: The background generated by the reactions in the counter telescope is larger than the signal. (The reason for this is probably obvious: In order to stop ^{10}Be and other fragments in the detector, it must necessarily be much thicker than the target.)

In the following are shown a number of examples of longitudinal energy spectra and energy-integrated angular distributions. For the latter, the cut in energy was from 26 to 80 MeV laboratory energy corresponding to a broad window around the mid-target beam energy of 41 MeV/u. The energy spectra of the forward neutrons shown later are

a proof that the combined selection of a fast neutron together with a ^{10}Be fragment leads to clean events that are not sensitive to the exact setting of the neutron-energy window. As a further test we also performed the analysis with the lower cut placed at 5 MeV; this leaves the results at low angles essentially unchanged but adds a nearly isotropic component beyond 20^0, which we interpret as the tail of a neutron spectrum arising from evaporation and from deep-inelastic processes. A few misplaced events corresponding to the collision of the ^{10}Be core with the target can make themselves strongly felt because of the large multiplicities possible at high excitation energy. With the lower cut set at 26 MeV and despite the very performant detector system, the measured differential energy-integrated cross sections to be discussed in the following were all smaller than 0.01 b/sr beyond 70^0 and consistent with zero.

3. Reactions of ^{11}Be: Theoretical Estimates

In the following are presented two sets of theoretical estimates that later will be compared with the experimental data. The first is a calculation of Coulomb excitation to the continuum in a perturbation treatment. The second is based on the sudden approximation and describes the combined effect of Coulomb and nuclear dissociation. In both cases it turns out to be possible to give analytical expressions describing the reaction amplitudes and the momentum distributions of the neutrons. There is no attempt to "fit" the data; our estimates of cross-sections are on an absolute scale and contain no free parameters[1].

3.1 STRUCTURE OF ^{11}Be AND REACTIONS OF HALO NUCLEI

The ground state of ^{11}Be, bound by a mere 0.504 MeV against break-up into ^{10}Be and a neutron, is notorious [30,31] for being predominantly a $1s_{1/2}$ intruder state instead of the $0p_{1/2}$ state that the simple shell model would predict for the seventh neutron. The latter state is found at 0.320 MeV; its large transition probability for the E1 gamma ray to the ground state was an early experimental indication of the halo and was correctly interpreted in terms of the large spatial dimensions of these states [32].

Additional states have been observed as resonances in ^{9}Be(t,p) and ^{10}Be(d,p) reactions [31], most of them as broad (Γ=0.1-0.3 MeV) resonances. The beta decay of ^{11}Li could in principle also give information on the ^{11}Be resonances, but the beta strength function is difficult to study because of a strong population of many broad final states, some of which have complex decays. More recently, also the ^{11}B(d,^{2}He) charge-exchange

---

[1] As mentioned earlier our experimental data are also quoted on an absolute scale. Regrettably, a number of experimental an theoretical papers on the subject present their results in "arbitrary units". We believe that a quantitative approach gives a better answer to the question, whether the essential features of the reaction are understood.

reaction has been studied [33]. However, since the halo structure is a threshold phenomenon, one cannot expect that the study of other states in the same nucleus has any special relevance to the halo, such as assumed in [33].

Several theoretical papers have discussed the properties and structure of the ground state of ^{11}Be. A generally recognized ingredient for all halo nuclei is that the halo is the result of a low one- or two-neutron separation energy, which by quantum-mechanical tunneling gives rise to a thin "neutron stratosphere" [34,35]. Since the balance is so delicate it becomes necessary to constrain the calculations so that they reproduce the experimental neutron separation energy. The isotope ^{11}Be was investigated by Hoshino et al. [36], who used a Hartree-Fock (HF) model to compare the roles of the two phenomena that are characteristic to ^{10}Be: (i) configuration mixing (leading to the appearance of the $s_{1/2}$ intruder state as the ground state), and (ii) the low neutron separation energy. They concluded that the latter was responsible for the large increase in matter radius. Density distributions and *rms* radii were calculated by Sagawa [17], who also pointed out that only states with orbital angular momenta less than or equal to unity were "likely to be halo configurations". This is an illustration of a general theorem [37] valid for short-range potentials. Otsuka et al. [38] have used a variational technique and find a neutron density of about 10^{-5} fm^{-3} at a distance of 10 fm in good agreement with the results of Sagawa. They find that the microscopic wave function is mainly $s_{1/2}$ with some $d_{5/2}$ coupled to the 2^+ state of ^{10}Be. This agrees well with the experimentally determined l=0 spectroscopic factor [30] of 0.73±0.06. We noted in our previous paper [23] that both for Coulomb and for nuclear processes involving the halo it is sufficient to use a wave function that describes its outer tail correctly. We outline in sub-section 3.2 the approximations that we have adopted to this end.

There is a considerable literature on the subject of reactions of halo nuclei, see the reviews [1-8]. The dissociation reactions on heavy targets are dominated by Coulomb excitation directly to the continuum and the calculations are especially simple [39] for the relatively high beam energies involved here; the trajectories are nearly straight lines and perturbation theory is applicable [40-44]. In the preliminary account of our ^{11}Be experiment [23] it was shown that for the gold target the absolute cross section as well as the angular distribution could be accounted for in the standard perturbation theory of Coulomb excitation without any free parameters. We refer to this paper for a full comparison of experiment and theory but give for completeness in sub-section 3.3 the essential formulas.

In the long sub-section 3.4 we go beyond perturbation theory and present an analysis based on the sudden approximation. It includes

nuclear contributions, it accounts for Coulomb-nuclear interference, but it treats Coulomb excitation more cavalierly. The validity of this approach comes from the fact that the intrinsic velocity of the halo neutron is much lower than that of the beam. The second essential ingredients is that the dissociation reactions leading to ^{10}Be or (^{10}Be+n) as final products come essentially from collisions with impact parameter larger than a minimum value, taken to be the sum of the core and target radii

$$b_{min} = r_0 [(A_1-m)^{1/3}+A_2^{1/3}] \quad (1)$$

where m, A_1 and A_2 are the mass numbers of the halo (here unity), the projectile and the target and where r_0 is taken to be 1.25 fm. The point, once again, is that collisions at shorter distances will lead to disintegration of the projectile.

The angular distributions in the laboratory system were obtained as follows. First the angle and momentum coordinates of the emerging neutron were transformed back to the system moving with beam velocity. The cross-section was calculated in this and subsequently transformed back to the laboratory system. The results are shown in Section 4.

3.2 WAVE FUNCTIONS

In our first paper [23] on ^{11}Be dissociation the Coulomb cross-section was calculated in the framework of the usual perturbation treatment of Coulomb excitation. The process proceeds from a bound *1s* state to continuum *p* states. Two nuclear models were used, of which the first was a single-particle well-depth recipe based on a Woods-Saxon potential. The second model used the "zero-range approximation with a finite-size correction", referred to as (ZR), which we shall introduce in a moment. In spite of the simplicity of the latter model, the agreement with the former was found to be extremely good. The reason for this is that the main part of the transition probability comes from the tail of the halo wave function, which is almost identical in the two cases.

Because of its extreme convenience we shall use the ZR approximation for most of the estimates in the following. In this, the particle is held by a delta function potential, which has only one bound state, a 0s state in the notation used here, and characterized by a Yukawa wave function

$$\psi_0(\boldsymbol{r}) = \frac{1}{\sqrt{2\pi\rho}} \frac{\exp(-r/\rho)}{r} \quad (2)$$

where the decay length

$$\rho = \frac{\hbar}{\sqrt{2\mu S_n}} \quad (3)$$

is given in terms of the reduced mass and the neutron separation energy. This approximation gives the correct shape of the wave function at large

distances, but the absolute value is too small. The correction factor, which we refer to as a finite-size correction [34], can be approximated as

$$F = \exp(a/\rho) / (1+a/\rho)^{1/2} \qquad (4)$$

where agreement with calculations with a finite well such as described below is obtained if a is taken to be 2.31 *fm*. For processes that are dominated by the neutron wave function at large distances it is a useful improvement to augment the final reaction cross-section by a factor F^2. This has been done in all calculations in the following. (It is probably clear that if the correction were to be applied from the start, it would not be possible to exploit the normalization and completeness of the wave function.) In this paper the correction amounts to a factor 1.5.

For the calculations of the ground-state momentum distributions we used a 1s neutron bound in a square well potential with a depth adjusted to reproduce the experimental neutron separation energy of 0.504 MeV and with a well radius of 2.53 fm. The latter value was chosen from the requirement that the *rms* radius r_c of the halo neutron measured from the centre of mass should have the normal *p*-shell value of 2.5 fm if the neutron binding energy is 6 MeV. For ^{11}Be the relation is $\langle r_c^2 \rangle = 10\langle r^2 \rangle/11$. Comparison of the wave function for the halo neutron obtained in this way with the more refined calculation by Sagawa [17], see the figure given in his paper, shows almost exact agreement for the outer part and a good degree of resemblance for the inner part.

3.3 COULOMB EXCITATION

The zero-range approximation has been used extensively by Baur, Bertulani and Canto, whom we follow here, see [40,42,43] and also the recent review [4]. In perturbation theory the Coulomb excitation of the neutron halo is predominantly *E1* leading to the *p* part of the plane wave states, and the double-differential cross-section in the projectile coordinate system can be written in closed form

$$\frac{d^2\sigma}{d\Omega k^2 dk} = \frac{16\rho^5}{\pi}\left(\frac{\alpha Z_1 Z_2 m}{A_1 \beta}\right)^2 F^2 A(k)\, B(\vartheta, \xi) \qquad (5)$$

with Z_1,Z_2 are the charges of the projectile and target, m,A_1 the mass numbers of halo and projectile, and β the projectile velocity in units of the speed of light c. The functions are defined as

$$A(k) = \frac{\rho^2 k^2}{(1+\rho^2 k^2)^4} \qquad (6)$$

with k denoting the wave vector in the centre-of-mass system of the halo nucleus (reduced mass μ), and

$$B(\vartheta,\xi) = \frac{\xi^2(K_1^2-K_0^2)}{\gamma^2} + \left[\xi K_0 K_1 - (\frac{3}{2}-\beta^2)\,\xi^2(K_1^2-K_0^2)\right]\sin^2\vartheta \qquad (7)$$

where ϑ is the neutron angle relative to the beam axis and γ the Lorentz factor. Integration over the angle ϑ leads to the expression given by Bertulani and Baur [40] for the differential cross-section (their eq. 4.3b; note that the constant should be 128/3, see also [4]). The argument of the modified Bessel functions is the parameter

$$\xi = \frac{(\hbar^2k^2/2\mu + S_n)\; b_{min}\;(1+\varepsilon_C)}{\hbar c\gamma\beta} \qquad (8)$$

where the term in ε_C is a correction for Coulomb deflection of the projectile (see [39,44]) and the minimum impact parameter was defined in (1).

3.4 DIFFRACTION AND COULOMB DISSOCIATION IN THE SUDDEN APPROXIMATION

For the beryllium (^{9}Be) target, our previous paper [23] found that the Coulomb contribution was much too small to account for the measured cross angular distribution, which furthermore had the broad angular shape characteristic of diffraction. The magnitude of the nuclear dissociation cross-section, also for ^{11}Li [10], could be understood from a geometrical model originally proposed by Glauber [21] for calculating the cross-sections for break-up of the deuteron, see also the alternative presentation given in Landau and Lifshitz [45]. The model was extended [23] to give momentum distributions of the outgoing neutrons, and in the following it is extended further to include also the Coulomb contribution, so that one and the same theory is applied to light and heavy target nuclei.

The calculation is based on a number of assumptions, (i) straight-line trajectories, (ii) the sudden approximation, valid since the projectile velocity is much larger than the intrinsic velocity of the halo neutron, (iii) the neglect of final-state interactions, (iv) the tail of the halo is well developed, (v) the target nucleus can be approximated by a "black disc", so that a neutron scattered or absorbed in the target is removed from the cross-sections that we consider, and, (vi) that there is only one bound state of the system, the ground state, which means that the $1/2^-$ excited level at 320 keV is neglected[1]. This last assumption allows us to use the completeness of the wave functions to calculate transition probabilities to the continuum, a treatment that is equivalent to the use of a (non-energy weighted) sum rule. Finally, (vii) only the transverse part of the Coulomb impact is taken into account (it is the dominant contribution).

---

[1] The contribution is not negligible. From its known E1 transition probability, it can be estimated that the Coulomb excitation cross-section of this state under the conditions of the experiment would have a cross-section of the order of 20% of that leading to the continuum.

The break-up probability will vary as b^{-2}, where b is the impact parameter, thus giving a logarithmic divergence in the total cross-section. The remedy for this is the usual practice (viii) of limiting the integration over impact parameter to an outer cut-off radius that can be obtained by comparing the total cross-section with the limiting form of that calculated in perturbation theory, eq. (7). In terms of the relativistic parameters β,γ the outer cut-off is at

$$b_{max} = 1.123\,\beta\gamma \exp(-\beta^2/2)\,\frac{\hbar c}{2S_n} \qquad (9)$$

see e.g. [4,40]. Here the numerical factor represents the constant $2/e^{\gamma}$, where γ here and only here denotes the Euler constant 0.577. Under the conditions of the ^{11}Be experiment the outer ("adiabatic") cut-off limit is 63.5 fm, much larger than the decay length of 3.4 fm for the Yukawa density, so the nuclear integrals will converge correctly with this approximation.

3.4.1 *Dissociation cross-sections.* Consider now a coordinate system CM situated in the centre-of-mass of the system ^{10}Be+n and travelling with beam velocity $\beta=v/c$ along the z axis. With the impact parameter $\boldsymbol{b}$ along the positive x axis the recoil wave vector imparted to the charged core due to the Coulomb force is

$$\boldsymbol{Q} = -\frac{\boldsymbol{b}}{b^2}\,\frac{2Z_1Z_2e^2}{\hbar c\beta} \qquad (10)$$

where the Coulomb deflection and also the longitudinal component have been neglected. In the new centre-of-mass system CM' after the collision the wave vector of the neutron is $\boldsymbol{q}=-\boldsymbol{Q}m/A_1$, the mass number m of the halo being unity for ^{11}Be.

At the same time the target nucleus has swept through the halo and has left a "wound" $\delta\psi_0$, with value ψ_0 inside the tube swept by the target and zero outside, see Fig. 4, so that the wave function in CM' after the collision can be approximated by

$$\psi(\boldsymbol{r}) = \exp(i\boldsymbol{q}\cdot\boldsymbol{r})\cdot(\psi_0(r) - \delta\psi_0(\boldsymbol{r})) \qquad (11)$$

where the probability content of the wound, i.e. the probability of absorption of the neutron, is

$$P_a = \int |\,\delta\psi_0\,|^2\,d\tau \qquad (12)$$

corresponding to a normalization of the wave function after the collision to $1-P_a$. It is probably useful to underline that the word "absorption" refers to the context of a black-disc model and that we take it as representing neutrons deflected from forward propagation with essentially

beam velocity. Here and in the following it is convenient to keep track of the reaction channels by using wave functions normalized to absolute probability. The amplitude for an elastic process is the overlap of the wave function of the reaction complex eq. (11) with that of the ground state

$$\gamma_{el} = \int \psi_0^*(r)\,\psi(\boldsymbol{r})\,d\tau = \gamma_C - \gamma_{C+N} \tag{13}$$

thus leading to a Coulomb term and a Coulomb-plus-nuclear term. The probability P_{el} of an elastic process is the square of this quantity. We can now calculate the probability of an inelastic process

$$P_{inel} = 1 - P_a - |\gamma_{el}|^2 \tag{14}$$

which because of the assumption of only one bound state must represent transitions of a neutron to the continuum. With the normalization chosen here the probabilities can be converted to cross-sections by integration over the impact parameter $\boldsymbol{b}$ with volume element $2\pi bdb$.

In [10,23] the "wound" was in the form of a circular cylinder with radius chosen to reproduce the 0^0 cross-sections for free neutrons, see Fig. 4. This also introduces the simpler approximation used in the present paper, a planar cut-off at the x-coordinate $b_1=b-R_2$, where R_2 is the radius of the target nucleus. The reaction amplitudes can then be expressed analytically, so that that of the Coulomb interaction becomes

$$\gamma_C = \int \psi_0^*(r)\,e^{iqx}\psi_0(r)\,d\tau = \frac{\arctan(\rho q/2)}{\rho q/2} \tag{15}$$

and the nuclear and Coulomb terms are

$$P_a = \frac{1}{2}\exp(-2b_1/\rho) - \frac{b_1}{\rho}E_1(2b_1/\rho) \tag{16}$$

and

$$\gamma_{C+N} = \frac{E_1(\frac{2b_1}{\rho} - ib_1q) - e^{ib_1q}E_1(\frac{2b_1}{\rho})}{iq\rho} \tag{17}$$

where E_1 denotes the complex or real exponential integral. The cross-sections obtained by numerical integration of P_a and P_{inel} over impact parameter are given in Table 1.

3.4.2 *The momentum distributions.* The wave function (11) of the reaction complex is a superposition of the ground-state wave function and a mixture of excited states. Therefore its momentum distribution does not represent that of the outgoing neutrons. We may obtain an estimate of this by projecting out the ground-state wave function in the coordinate system CM' to obtain $\psi - \gamma_{el}\psi_0$, which clearly is orthogonal to ψ_0. This is transformed back to CM to obtain the decaying state in the coordinate system travelling with the beam

$$\psi_d(\boldsymbol{r}) = \psi_0(r) - \delta\psi_0(\boldsymbol{r}) - \gamma_{el}\exp(-i\boldsymbol{q}\cdot\boldsymbol{r})\,\psi_0(r) \qquad (18)$$

an expression, which has the correct normalization given by (14). As final-state interactions are neglected, the momentum distribution in CM is now obtained as the square of the Fourier transform of this expression.

The Fourier transform as a function of the wave vector $\boldsymbol{k}$ can be obtained analytically and is the sum of the following three terms correponding to the three terms in (18)

$$A_0 = \frac{\rho^{3/2}}{\pi(1+\rho^2 k^2)} \qquad (19)$$

and

$$A_\delta(\boldsymbol{k}) = -\frac{\rho^{3/2}}{2\pi\sqrt{1+\rho^2(k_y^2+k_z^2)}}\;\frac{\exp\left(-\frac{b_1}{\rho}\left[i\rho k_x+\sqrt{1+\rho^2(k_y^2+k_z^2)}\right]\right)}{i\rho k_x+\sqrt{1+\rho^2(k_y^2+k_z^2)}} \qquad (20)$$

where we have used Cartesian coordinates, and finally the Coulomb-plus-nuclear term, which is

$$A_{C+N}(\boldsymbol{k}) = -\gamma_{el}\frac{\rho^{3/2}}{\pi(1+\rho^2(\boldsymbol{k}+\boldsymbol{q})^2)} \qquad (21)$$

where the wave vector $\mathbf{q}$ is along the x axis. The differential cross-section in the coordinate system following the beam is obtained by integrating the square of the Fourier transform with the volume element $d\varphi b db$, where φ represents the azimuthal angle.

We finally note that the Coulomb excitation calculation based on the sudden approximation is consistent with the perturbation theory results of sub-section 3.3. Leaving out the nuclear terms and expanding eq. (21) in the quantity $q\rho<<1$ one obtains an expression for the differential Coulomb ceoss-section exactly identical with eq. (5) except that eq. (7) is replaced by

$$B(\vartheta,\xi) = \ln(b_{max}/b_{min})\,\sin^2\vartheta \qquad (22)$$

which has the same form as the leading term in the expansion of the Bessel functions in eq. (7). This result illustrates that the sudden approximation neglects the longitudinal term, proportional to $\cos^2(\vartheta)$, implicitly contained in eq. (7). The absence of this term is mainly felt at small angles, for which the sudden approximation underestimates the cross-section.

4. The Experimental Results

In the following the experimental cross-sections and distributions are compared with the theoretical estimates. The graphs show the data

with their statistical errors. Some of the points represent weighted averages over data from several detectors representing the same angle. On all the absolute neutron cross-sections there is in addition a general scale error stemming from the uncertainty of the detector efficiency, which we estimate to be ±20%.

The large spatial extension of the neutron halo is associated with small momentum components in its ground-state wave function. The data clearly show that these may survive after the reaction with some modifications coming from the reaction mechanism. One clear exception to this is diffraction dissociation on a light target, in which case the quasi-free halo neutron will give an inner diffraction peak [10] corresponding to an angle of the order

$$\vartheta_{1/2}=\frac{1.616}{k_B R_2} \qquad (23)$$

thus reflecting only the beam wave vector and the effective size of the target nucleus so that the width yields no information about the halo. (But the magnitude of the cross-section does.) We have shown [23] that the exclusive data for the beryllium target can be interpreted in this way.

For the other reactions than diffraction, the distributions in angle and in parallel momenta are expected to provide the most characteristic halo signatures at low momentum transfer to the outgoing neutron, say, below 100 MeV/c corresponding roughly to the nuclear size. With a beam momentum of 279 MeV/c/u this implies that the angles below 20^0 are the most interesting, and it was for this reason that the first discussion of the results [23] was limited to angles below 30^0. We show here the full data sets out to 70^0, the largest angle for which non-zero exclusive cross-sections could be detected. The information about large angles is, of course essential for all comparisons with integrated cross-sections, such as those from telescope data. However, the points at large angles do not necessarily have any direct relevance to the neutron halo.

The same is true *a fortiori* for the theoretical estimates developed above. They originate in a description of a halo nucleus in terms of a product wave function for the core and neutron and they cannot possibly give useful predictions of what happens at large momenta. We have, rather arbitrarily, chosen not to show the calculated angular distributions beyond 50^0. This is rather too much than too little: it corresponds to distances well below the size of the nucleus and approaching that of the nucleon. For a general discussion of distributions in radii and momenta of nucleons in nuclei we refer to the book by Antonov et al. [46].

4.1 THE SINGLE-NEUTRON EXCLUSIVE (n+^{10}Be) ANGULAR DISTRIBUTION

Fig. 5 shows the full exclusive angular distributions for the gold target. The main result, discussed already in [23], is that Coulomb excitation theory accounts well for the data at small angles and that it matters little whether the transition matrix element is calculated from a well-depth recipe or from a delta potential, such as is the case here. The sudden approximation also gives an acceptable degree of agreement except at the smallest angles, an effect discussed at the end of sub-section 3.4. The high momentum components (large angles) seem to be particularly well accounted for, but some of this may, of course, be an illusion created by our sharp cut-off at the target surface. The part of this cross-section that is caused by diffraction is shown separately. The contribution from interference will be discussed in sub-section 4.3. The (transformed) momentum distribution for a square well potential (marked 1*s*) is arbitrarily normalized to fit the points close to zero degrees, and it comes quite close to experiment. Qualitatively, at least, the notion that the experiments measure the momentum distribution of the ground-state is correct for a heavy target, and calculations show that this also true for other binding energies of the halo neutron. (Note, however that the Coulomb process "filters" the momentum components in such a way that the intensities at small and large angles are suppressed. The dip near 0^0 is the signature of the final *p* state.) This is an illustration of the statement by Esbensen and Bertsch [13] that "the dipole operator does not change the momentum content much".

Fig. 6 shows the exclusive data for the titanium and beryllium targets with the full-drawn lines representing the calculation in the sudden approximation. For the case of the titanium target the inclusion of the nuclear contributions improves the agreement as compared with the pure Coulomb calculation shown in [23]. The Coulomb contribution is negligible for the beryllium target. For this it is seen that the sudden approximation with the planar cut-off overestimates the intensity at small angles and creates a peak that is not present in the experiment. Better results were obtained with a more elaborate approximation [23] based on a cylindrical "wound" and neglect of Coulomb contributions. This is in support of the interpretation of the dissociation reaction on beryllium as a diffractive phenomenon and suggests (but does not prove) an approximate dependence on target size similar to the free-neutron estimate given in eq. (23).

4.2 THE SINGLE-NEUTRON EXCLUSIVE PARALLEL MOMENTUM DISTRIBUTION (n+^{10}Be)

It has been shown by Orr et al. [11] that the longitudinal momentum distribution of the core recoil is a sensitive tool for investigating momentum distributions. Whereas the transverse momentum distributions are smeared by Coulomb deflection, the Coulomb effects from the

ingoing and outgoing legs of the trajectory to a very good approximation cancel in the longitudinal distribution. The nuclear effects on the longitudinal distribution are small; as can be seen from eq. (20) the diffraction mechanism imparts transverse momentum, and the momentum distribution in the forward direction is close to that of the ground-state wave function.

4.2.1 *The longitudinal energy spectra of the neutrons.* The energy spectra in the forward direction should convey similar information as the experiments with core recoils, but our experimental set up was not optimized for this purpose. Wishing to emphasize the angular information, we had chosen to place a high-granularity array of small detectors at 0^0 (Fig. 1). Their correspondingly low detection efficiency leads to low statistics on the double-differential cross-sections; only the gold data are interesting enough to be shown. The results (Figs. 7 and 8) are in good agreement with the predictions of Coulomb excitation theory, especially when it is remembered that the curves are not adjusted fits but calculations on an absolute scale. It would have been interesting to have had enough statistics to see the peculiar double-humped spectrum predicted for the detectors at 0^0 and 1.48^0, the signature of the dipole excitation to the *p*-wave continuum.

In the Coulomb-excitation theory, with which we compare here, the fragments are, apart from small phase-space effects, travelling with beam velocity. Figs. 7 and 8 show that this is the case to a relatively good approximation, but it is possible that deviations could emerge under closer scrutiny. Since these would be an interesting tool for probing more deeply into the reaction mechanisms of halo nuclei we devote in the following sub-section some comments to this, still very speculative, topic.

4.2.2 *Pre-break-up Coulomb deceleration?* It is possible that the Coulomb interaction between a high-Z target and the outgoing fragments from Coulomb break-up will change their relative velocities in an important way. Such effects have been discussed theoretically for halo nuclei by Baur et al. [47] and by Bertsch and Bertulani [48], who both point out that the shifts may be an interesting tool for understanding the reaction mechanism, "a clock to measure the time it takes for the system to break up". But even apart from this, an understanding of the Coulomb final-state interaction is necessary for the interpretation of experiments, for example those in which it is attempted to measure radiative capture cross-sections via the inverse process of electrodissociation, see e.g. the papers by Baur et al. and by Kiener et al. [49,50].

There seems to be general consensus from a theoretical point of view that such effects are not expected to be important for the loosely bound halo systems at beam energies of tens of MeV/u. Qualitatively, this is because the collision time is shorter than the characteristic time of the

halo disintegration by roughly an order of magnitude. This implies that the halo nucleus breaks up at large distances and that the Coulomb shifts are small. This is also what the calculations by Baur and his collaborators and the recent paper by Canto et al. find [47,51,52]. Similar theories can correctly account for the observed large energy shifts found in the break up of relatively slow deuterons on heavy targets, see the work of Baur et al. [53]. To set a scale for the possible effects it is instructive to consider the following classical picture, which is qualitatively applicable to the case of slow deuterons just mentioned but hardly to the fast halo nuclei of our experiment.

Consider a slow-moving projectile that breaks up in the Coulomb field of a heavy target with charge Z_2. Let the excitation energy be high so that the halo neutron is separated instantaneously from the core. Assume furthermore a linear trajectory with impact parameter b and that break-up occurs at minimum distance to the nucleus. Then the energy of the outgoing neutron is changed by

$$\Delta E_n = -\frac{Z_1 Z_2 e^2}{A_1 b} \tag{24}$$

whereas the core is re-accelerated on the outgoing leg of the trajectory and, being lighter, emerges with an energy per nucleon increased by

$$\Delta E_C = \frac{Z_1 Z_2 e^2}{A_1 b} \cdot \frac{m}{(A_1 - m)} \tag{25}$$

where m (here equal to 1) is the mass number of the halo, so that the shift is numerically smaller than that of the neutron by an order of magnitude. The magnitude of the effect can be estimated by remembering that the break-up probability scales approximately as the square of eq. (10) and hence with b^{-2} so that the average shift is obtained by replacing b with

$$b_{eff} = \frac{\ln \frac{b_{max}}{b_{min}}}{b_{min}^{-1} - b_{max}^{-1}} \tag{26}$$

of the order of 20 fm. For our experiment this would correspond to a decrease of the neutron energy of 2.1 MeV and for the core fragment an increase of 0.2 MeV/u.

Our data are hardly consistent with a downward shift, but the precision is not high enough to allow a firm conclusion. The weighted average energy in the forward direction is 44±4 MeV for the inner detectors (Fig. 7) as compared with a theoretical value based on the Coulomb calculation (Section 3.3) of 42 MeV, both averaged over the

interval 20-60 MeV/u. For the spectrum in Fig. 8 the average is 45±3 MeV with the theoretical value 41 MeV.

Non-zero shifts have been reported in other experiments. Riisager et al. [15] found that the neutrons from Coulomb dissociation of ^{11}Li on a gold target were downshifted by about three MeV relative to the average beam energy of 29 MeV/u. Since a similar shift was seen [5,15] from nickel and beryllium targets this cannot be taken as evidence for a Coulomb effect. The accurate complete kinematics experiment[1] of Sackett et al. [54], working at almost the same energy, found on a lead target a velocity shift (in units of c) between the average velocity of the neutrons and that of the core being -0.0080±0.0003. This is exactly what one would naively calculate from eqs. (24-26) and more than 80% of the effect would in this interpretation be due to the deceleration of the neutrons. Thus, the picture is not yet clear. The subject is one to follow.

4.3 THE DISSOCIATION CROSS-SECTIONS

Theoretical and experimental results are compared in Table 1. The Coulomb cross-sections are the integrals of the estimates in [23], which neglected nuclear contributions and hence represent a pure dissociation process. The integrals of the experimental exclusive neutron cross sections between 0^0 and 20^0 show that the Coulomb contribution can account for essentially all of the gold cross-section at small angles, for half of the titanium cross-section and for 6% of the beryllium cross-section.

The calculations based on the sudden approximation include processes in which the halo neutron collides with the target nucleus. In the black-disc picture that is used here, the hard collisions of the neutron with the core are represented by "absorption", and we call the corresponding cross-section σ_a the absorption cross-section. This term should not be taken literally; what is meant is that the neutron will not appear in the forward direction with essentially beam velocity. The other nuclear process is diffraction dissociation, which excites the neutron to low-lying states in the continuum, and hence represents an inelastic process. In the theory of reactions of free neutrons, the absorption and diffraction mechanisms give identical contributions in the black-disc model leading to the well-known result that the total neutron cross-section for neutrons in the MeV range is twice the geometrical cross-section. The calculation for the beryllium target shows that the same relationship holds for the halo nuclei in the absence of Coulomb effects; it is easy to prove that the relation is exact in the limit of small absorption probability P_a.

---

[1] Note, however, that the epithet "complete" here refers to the reconstruction of the observed events. The geometrical acceptance of the neutron hodoscope limited the sample of the coincidences to roughly 10% of the most central events. This effect was incorporated into the theoretical analysis by Canto et al. [52].

For the heavier targets the nuclear and Coulomb inelastic processes contribute coherently to the inelastic channel. The interference is destructive but not very important, as can be seen by repeating the calculation in the sudden approximation with the Coulomb or the nuclear terms set to zero. The sum of these two cross-sections exceeds the calculation of the combined effect by 1, 6 and 10% for the three targets Be, Ti and Au, respectively. This agrees well with an estimate of 5% Coulomb interference for a heavy target made by Bertulani et al. [4].

The calculated total cross-sections for (^{11}Be,^{10}Be) are obtained as the sum of the absorptive and inelastic contributions; they agree well with the results from the telescope measurements shown on the line below in Table 1. The calculated inelastic cross-sections also agree well with the integrals of the measured single-neutron exclusive cross-sections for the range observed (0^0 to 97^0, but no signal was, in fact, seen beyond 70^0). The general trend in calculated and measured cross-sections is illustrated in Fig. 9. The agreement is seen to be good.

The ratios of the integrated exclusive neutron cross-sections to the telescope data give, just as for ^{11}Li in [10], the average multiplicities, which, however have too large errors to furnish a good check on our interpretation. The agreement is respectable for the gold target, for which the experimental value in barn is 1.02±0.28 (theory σ_{inel}/σ = 0.90), and marginal for Ti with 0.85±0.21 (0.67) and for Be with 0.83±0.21 (0.5).

The data of Table 1 are displayed in Fig. 9, which shows that the Z_2 dependence of the cross-sections is well accounted for by the three mechanisms incorporated in our theory. This is probably a good occasion to comment on a number of previous attempts to split total cross-sections empirically into a nuclear and a Coulomb part and on the associated question of how the electric part of the cross-section scales as a function of Z_2. Kobayashi et al. [55] assumed that the dissociation cross-section for ^{11}Li was proportional to the sum of the core and target radii, something that agrees well with the absorption cross-section shown in Fig. 9. They found that the remaining Coulomb cross-section scaled as Z_2 to the power 1.41±0.22, while our theoretical curve for ^{11}Be after subtraction of the nuclear part corresponds to the power 1.92, and our experimental data would give the power 1.57±0.32, also after subtraction of a nuclear part extrapolated from the beryllium point.

There are several reasons why the Coulomb part inferred from experimental data should not scale as Z_2^2. As already mentioned above, one contribution comes from Coulomb-nuclear interference, which for the gold target amounts to a 10% reduction. Furthermore, the inner cut-off in the impact parameter implies an approximately logarithmic dependence of the Coulomb cross-section on the sum of the core and target radii; relative to titanium a gold target will for this reason have the

extrapolated cross-section reduced by 13%. And, finally, for the small impact parameters the E1 excitation amplitudes are so high that they approach unity and consequently deviations from perturbation theory are to be expected. Since our treatment based on the sudden approximation does not assume perturbation theory (but contains its leading term as a limit valid for low Z_1Z_2 and high velocities, see the remarks at the end of sub-section 3.4.2) we can test this effect by replacing the arctangent in eq. (15) by the two first terms of its series expansion. Considering only the Coulomb effect, we find for a gold target that perturbation theory gives a cross-section that is 4% larger than what is obtained from the "exact" calculation. The last two effects have been discussed by Soutome et al. [56] as an explanation for the scaling law found for ^{11}Li.

4.4 THE RESTRICTED INCLUSIVE CROSS-SECTIONS

The compact geometry of the target-telescope arrangement (Fig. 1) was in sub-section 2.3 called the Achilles' heel of our experimental technique, but it also has its rewards. Since the heavy fragments from break-up of the projectile core all are recorded in the counter telescope, it is possible, as described in the introduction to Sect. 2, to introduce an anti-coincidence requirement. Instead of showing angular distributions of the single-neutron inclusive events as was done in our first paper [23], we can remove from those all events already contained in the dissociation cross-sections. The remaining complement is what we refer to as "restricted inclusive cross-sections", thus corresponding to the channel "single neutron plus anything different from ^{10}Be". The corresponding angular distributions are shown for the beryllium and titanium targets as the top line of experimental points in Figs. 10 and 11. The results for the gold target were very similar in absolute magnitude, but had much inferior statistics.

We believe that with the one-neutron removal reactions taken out of the data, the remaining events must be characteristic of core-target collisions, and we interpret them as arising from encounters with impact parameters smaller than the sum of the core and target radii. Another appropriate name to describe this category of events would be "core removal reactions". The angular and energy distributions of neutrons, protons and other fragments arising from such fragmentation and deep-inelastic events have been studied in a number of cases, and the results are quite complex. There would at first sight seem little hope to learn much from events of this type, but there are, in our view, three arguments why such studies may convey useful information about a simple structure such as the neutron halo.

(i) We note first of all that a halo neutron has a probability distribution that extends far beyond the core and that as a consequence it must have an appreciable probability of going clear of the debris from the core-target conflagration. This is an obvious case for the sudden

approximation: The neutron viewed in the coordinate system following the beam should, as in Serber's model [20] of the deuteron break-up, emerge with a momentum distribution characteristic of the halo wave function. Under the right experimental conditions this could then permit a mapping of the Fourier transform of the halo wave function.

(ii) In order to correct for the neutrons arising from the debris, the experiment should then be repeated with the core (e.g. ^{10}Be) as a projectile and at the same beam velocity as that used for the halo nucleus. The difference would then reflect the contribution of the halo neutron. Still, it is necessary to consider the extent to which more complex neutron-core scattering processes will contribute.

(iii) The data presented here seem to indicate that the neutrons arising from fragmentation are strongly suppressed when the velocity is selected to be close to that of the beam. The total cross-sections for the restricted inclusive reactions shown in Table 1 are much smaller than what would be expected from the geometrical cross-sections multiplied by a large multiplicity. This is a hint that the target absorbs or retards the fast neutrons from fragmentation and that the halo neutrons contribute an appreciable part of the absolute cross-section.

Let us now consider the extent to which the data support the interpretations just given. The absolute cross-sections for restricted inclusive neutron events in Table 1 are not very precise, but they vary so little with the target mass that an interpretation in terms of a shadowing effect given in (iii) seems justified. The shapes of the angular distributions are the same for the beryllium and titanium targets and furthermore the two figures 10 and 11 show that essentially identical shapes emerge for exclusive events involving outgoing helium and lithium ions, fragmentation products of the projectile core. All this is consistent with fragmentation processes occurring mainly in the periphery of the target nuclei.

The angular distributions of Fig. 10 and 11 have a shape that seems to indicate a superposition of a narrow and a broad component, where the former could be the one that we associate with the halo neutron. The figures also show the theoretical momentum distribution of a 1*s* state of a finite well. The good agreement with the measured shape at small angles gives further support to our interpretation. It is also possible to make a semi-quantitative estimate to check whether the scale is reasonable. We have used the geometrical model of Fig. 4 (with the cylindrical wound) to calculate the probability that the halo neutron goes clear of the core-target collision complex. After integration over the impact parameter going from zero to the sum of the radii, we obtain an estimated cross-section coming from the halo neutron of 0.5 *b* for the beryllium target and 1.1 *b* for the gold target. This is somewhat smaller

than the integrated experimental cross-sections given in Table 1, but these also contain neutrons from fragmentation. The fragmentation part is not easily calculated but could have been measured in a separate run with ^{10}Be as the projectile.

The results suggest that one might find the true momentum distribution of the halo by subtracting from the restricted inclusive neutron distribution that measured with the core as the projectile. The pairs ^{11,10}Be and ^{11,9}Li are obvious candidates for an experiment of this kind, which we plan to carry out in the near future. It is clear that the angular distributions will be altered somewhat by diffraction phenomena, but the longitudinal distributions are also easy to measure and should be cleaner.

5. Concluding Remarks

The experiments have shown that dissociation reactions of ^{11}Be (*i.e.* those that leave the ^{10}Be core intact) are dominated by the neutron halo and that all cross-sections can be understood in a quantitative way that conveys information about the halo structure. The hope in much of the work of this kind was originally to use the momentum distributions of the fragments to reconstruct the halo wave function in momentum coordinates, and although we are approaching this goal, we at the same time realize that the results of most experiments arise from an interplay between halo structure and reaction mechanism.

Essentially every result discussed in Sect. 4 illustrates some aspect of this interplay and it is hardly necessary to mention them all again at this point. Instead let us give two striking examples. The first is that the distribution following Coulomb dissociation (Fig. 5) on a heavy target is not so far from representing the intrinsic momentum distribution. The narrow angular distribution is qualitatively the signal of a large source (the halo) but it is seen that it is modified at large and small momenta by contributions from the mechanism. The second example is the broad angular distribution from the beryllium target (Fig. 6) where the magnitude of the cross-section (see Table 1) is a clear halo signal, but where the shape only conveys the message that the target is small. This interpretation is supported by the fact that the model with the cylindrical cut-off works better than the model with the planar cut-off, which assumes infinite radius for ^{9}Be.

We had originally undertaken these experiments with the idea that the halo would be best investigated in gentle collisions at impact parameters greater than the sum of the core and target radii. It is certainly true that such reactions are specific to halo nuclei. But as outlined in sub-section 4.4 it could well be that important complementary information about the halo wave function in momentum coordinates

eventually will emerge from the violent core-target fragmentation events for which the sudden approximation works well.

During the analysis of the experiment we have benefitted from assistance and advice from Gerhard Baur, Aksel S. Jensen, Geoffrey C. Oades, and Jan S. Vaagen to whom our best thanks are due. The use of the neutron detectors from NORDBALL and the MSI (Uppsala) was facilitated by the help given to us by Örjan Skeppstedt and Geirr Sletten. And, finally, the external members of our collaboration would like to express their appreciation of the friendly reception and user-efficient services that they have enjoyed at GANIL.

References

[1] I. Tanihata, Nucl. Phys. **A520** (1990) 411c and **A522** (1991) 275c.

[2] T. Kobayashi, Nucl. Phys. **A538** (1992) 343c and **A553** (1993) 465c.

[3] P.G. Hansen, Nucl. Phys. **A553** (1993) 89c.

[4] C.A. Bertulani, L.F. Canto and M.S. Hussein, Phys. Reports **226** (1993) 281-378.

[5] K. Riisager, Residence in forbidden regions (dissertation presented for the Dr. Scient. degree, Aarhus University 1993), to be published.

[6] M.V. Zhukov, B.V. Danilin, D.V. Fedorov, J.M. Bang, I.J. Thompson and J.S. Vaagen, Physics Reports **231** (1993) 151-199.

[7] A.C. Mueller and B.M. Sherill, Nuclei at the limits of particle stability, to appear in Ann. Rev. Nucl. and Part. Sci. **43** (1993).

[8] B. Jonson, Halo nuclei, to be published in Proc. Int. Conf. on Perspectives in Nuclear Structure, Nucl. Phys A (in press).

[9] T. Kobayashi, O. Yamakawa, K. Omata, K. Sugimoto, T. Shimoda, N. Takahashi and I. Tanihata, Phys. Rev. Lett. **60** (1988) 2599.

[10] R. Anne, S.E. Arnell, R. Bimbot, H. Emling, D. Guillemaud-Mueller, P.G. Hansen, L. Johannsen, B. Jonson, M. Lewitowicz, S. Mattsson, A.C. Mueller, R. Neugart, G. Nyman, F. Pougheon, A. Richter, K. Riisager, M.G. Saint-Laurent, G. Schrieder, O. Sorlin and K. Wilhelmsen, Phys. Lett. **B250** (1990) 19.

[11] N.A. Orr, N. Anantaraman, Sam M. Austin, C.A. Bertulani, K. Hanold, J.H. Kelley, D.J. Morrisey, B.M. Sherrill, G.A. Souliotis, M. Thoennessen, J.S. Winfield and J.A. Winger, Phys. Rev. Lett. **69** (1992) 2050.

[12] J. Hüfner and M.C. Nemes, Phys. Rev. **C23** (1981) 2538.

[13] H. Esbensen and G.F. Bertsch, Nucl. Phys. **A542** (1992) 310.

[14] F. Barranco, E. Vigezzi and R.A. Broglia, Nuclear effects in the break-up of ^{11}Li, to be published.

[15] K. Riisager, R. Anne, S.E. Arnell, R. Bimbot, H. Emling, D. Guillemaud-Mueller, P.G. Hansen, L. Johannsen, B. Jonson, A. Latimier, M. Lewitowicz, S. Mattsson, A.C. Mueller, R. Neugart, G. Nyman, F. Pougheon, A. Richard, A. Richter, M.G. Saint-Laurent, G. Schrieder, O. Sorlin and K. Wilhelmsen, Nuclear Physics **A540** (1992) 365.

[16] C.W. de Jager, H. de Vries and C. de Vries, Atomic Data and Nucl. Data Tables **14** (1974) 486.

[17] H. Sagawa, Phys. Lett. **B286** (1992) 7.

[18] J.R. Oppenheimer, Phys. Rev. **47** (1935) 845.

[19] S.M. Dancoff, Phys. Rev. **72** (1947) 163.

[20] R. Serber, Phys. Rev. **72** (1947) 1008.

[21] R.J. Glauber, Phys.Rev. **99** (1955) 1515.

[22] G. Fäldt, Phys. Rev. **D5** (1970) 846.

[23] R. Anne, S.E. Arnell, R. Bimbot, S. Dogny, H. Emling, H. Esbensen, D. Guillemaud-Mueller, P.G. Hansen, P. Hornshøj, F. Hum-

bert, B. Jonson, M. Keim, M. Lewitowicz, P. Møller, A.C. Mueller, R. Neugart, T. Nilsson, G. Nyman, F. Pougheon, K. Riisager, M.-G. Saint-Laurent, G. Schrieder, O. Sorlin, O. Tengblad, K. Wilhelmsen Rolander and D. Wolski, Phys. Lett. **B304** (1993) 55-59.

[24] S. Dogny, Etudes des réactions induites par un faisceau secondaire de ^{11}Be dans les cibles de Be, Ti et d'Au, Thèse d'Université, IPN-Orsay, report IPNO-T.92.03, October 1992.

[25] K. Wilhelmsen Rolander, Neutron Halo Nuclei, Ph.D. thesis, Chalmers, Gothenburg, October 1993.

[26] A.C. Mueller and R. Anne, Nucl. Instr. Meth. **B56** (1991) 559.

[27] F. Hubert, R. Bimbot and H. Gauvin, Atomic Data and Nuclear Data Tables **46** (1990) 1.

[28] R.A. Cecil, B.D. Anderson and R. Mady, Nucl. Instr. Meth. **161** (1979) 439.

[29] M. Cronqvist, B. Jonson, T. Nilsson, G. Nyman, K. Riisager, H.A. Roth, Ö. Skeppstedt, O. Tengblad and K. Wilhelmsen, Nucl. Instr. Meth. **A317** (1992) 273.

[30] F. Ajzenberg-Selove, Nucl. Phys. **A506** (1990) 2, 6-8.

[31] F. Ajzenberg-Selove and C.L. Busch, Nucl. Phys. **A336** (1980) 1.

[32] D.J. Millener, J.W. Olness, E.K. Warburton and S.S. Hanna, Phys. Rev. **C28** (1983) 497.

[33] H. Sakai, H. Okamura, S. Ishida, H. Okuno, N. Fukunishi, H. Sagawa, A. Okihana, Y. Nakai, T. Takeda, T. Toriyama and Y. Yoshida, Phys. Lett. **B302** (1993) 7.

[34] P.G. Hansen and B. Jonson, Europhys. Lett. 4 (1987) 409.

[35] G.F. Bertsch, B.A. Brown and H. Sagawa, Phys. Rev. **C39** (1989) 1154.

[36] T. Hoshino, H. Sagawa and A. Arima, Nucl. Phys. **A506** (1990) 271.

[37] K. Riisager, A.S. Jensen and P. Møller, Nucl. Phys. **A548** (1992) 393, D.V. Fedorov, A.S. Jensen and K. Riisager, Phys. Lett. **B312** (1993) 1 and to be published.

[38] T. Otsuka, N. Fukunishi and H. Sagawa, Phys. Rev. Lett. **70** (1993) 1385.

[39] Aa. Winther and K. Alder, Nucl. Phys. **A319** (1979) 518.

[40] C.A. Bertulani and G. Baur, Nucl. Phys. **A480** (1988) 615.

[41] C.A. Bertulani and G. Baur, Nucl. Phys. **A526** (1991) 751-761.

[42] G. Baur, in Structure and Reactions of Unstable Nuclei (K.Ikeda and Y. Suzuki eds.), World Scientific, Singapore 1991, p.211.

[43] C.A. Bertulani and L.F. Canto, Nucl. Phys. **A539** (1992) 163.

[44] H. Esbensen, Phys. Rev. **C44** (1991) 440.

[45] L.D. Landau and E.M. Lifshitz, Quantum Mechanics, Non-Relativistic Theory, 3rd edition (Pergamon, Oxford, 1977), p. 648.

[46] A.N. Antonov, P.E. Hodgson and I.Zh. Petkov, Nucleon momentum and density distributions, (Clarendon Press, Oxford, 1988), pp. 1-165.

[47] G. Baur, C.A. Bertulani and D.M. Kalassa, Nucl. Phys. **A550** (1992) 527.

[48] G.F. Bertsch and C.A. Bertulani, Nucl. Phys. **A556** (1993) 136.

[49] G. Baur, C.A. Bertulani and H. Rebel, Nucl. Phys. **A458** (1986) 188.

[50] J. Kiener, H.J. Gils, H. Rebel, S. Zagromski, G. Gsottschneider, N. Heide, H. Jelitto and G. Baur, Phys. Rev. **C44** (1991) 2195.

[51] R. Shyam, P. Banerjee and G. Baur, Nucl. Phys. **A540** (1992) 341.

[52] L.F. Canto, R. Donangelo, A. Romanelli and H. Schulz, A coupled channels study of ^{11}Li Coulomb dissociation, IF/UFRJ/93/08 and to be published.

[53] G.Baur, F. Rösel, D. Trautmann and R. Shyam, Phys. Repts. **111** (1984) 354.

[54] D. Sackett, K. Ieki, A. Galonsky, C.A. Bertulani, H. Esbensen, J.J. Kruse, W.G. Lynch, D.J. Morrisey, N.A. Orr, B.M. Sherill, H. Schulz, A. Sustich, J.A. Winger, F. Deák, A. Horváth, A. Kiss, Z. Seres, J.J. Kolata, R.E. Warner, and D.L. Humphrey, Phys. Rev **C48** (1993) 118.

[55] T. Kobayashi, S. Shimoura, I. Tanihata, K. Katori, K. Matsuta, T. Minamisono, K. Sugimoto, W. Müller, D.L. Olson, T.J.M. Symons and H. Wieman, Phys. Lett. **B232** (1989) 51.

[56] K. Soutome, S. Yamaji and M. Sano, Nucl. Phys. **A538** (1992) 383c and Prog. Theor. Phys. **88** (1992) 703.

Table 1

Theoretical and Experimental Cross-Sections in barn for ^{11}Be (41 MeV/u)

	Targets		
	Be	**Ti**	**Au**
1. Theory			
Coulomb Excitation[1)]	0.0074	0.19	2.02
Sudden Approximation[2)]			
σ_{abs}	0.18	0.22	0.29
σ_{inel}	0.18	0.44	2.68
$\sigma(^{11}Be, ^{10}Be)$	0.36	0.66	2.97
2. Experiment			
Telescope data			
$\sigma(^{11}Be, ^{10}Be)$	0.29±0.04	0.65±0.09	2.45±0.20
Neutron data[3)], exclusive			
$\int \frac{d\sigma_n}{d\Omega} d\Omega$ (^{11}Be, ^{10}Be+n)			
0 - 20^0	0.120±0.024	0.40±0.08	2.20±0.45
0 - 100^0	0.24±0.05	0.55±0.11	2.5±0.5
Neutron data[3)], restricted inclusive			
$\int \frac{d\sigma_n}{d\Omega} d\Omega$ (^{11}Be, n+X($\neq^{10}$Be))			
0 - 20^0	1.0±0.2	1.1±0.2	0.8±0.3
0 - 100^0	1.5±0.3	1.6±0.3	1.0±0.4

Footnotes to Table 1

1) Perturbation theory; zero-range wave function with finite-size correction.

2) Coulomb and diffraction dissociation in planar cut-off model. The cylindrical cut-off used in [23] and in Fig.6 gave for the Be target $\sigma_{abs} = \sigma_{inel} = 0.16$.

3) The errors are here essentially the (fixed) ± 20% error on the absolute calibration. The neutron energy window is 26 - 80 MeV.

Captions

Fig 1
The experimental arrangement. In the foreground is seen the end of the LISE3 beam line and the reaction chamber containing the target and counter-telescope sandwich (inset). At 3 m distance from the target and covering angles from -32^0 to 97^0 were placed an 32 liquid scintillation detectors (BC 501) of different sizes. In order to have high granularity near 0^0 the range out to 4.4^0 was covered with 9 small scintillators 5 cm dia. and 10 cm long and centered on the beam axis. The array extended out to 97^0 with larger detectors (15 cm thick and 7, 8 and 30 cm dia.); some of the large detectors were placed at smaller angles, the first at -9^0, to provide sensitivity to rare events.

Fig. 2
Ion energy spectra as a function of E_3 (arbitrary scale) measured in the particle telescope and in coincidence with neutrons. For each of the three targets, the background with the empty target frame (i.e reactions in the silicon detectors) and normalized to the same number of incoming projectiles is shown as an overlay. The ^{11}Be peak is due to a small fraction of random coincidences, which we have not corrected for. It is seen that the reactions with gold are essentially (Coulomb) dissociation reactions leading to ^{10}Be. For the Ti and Be targets (nuclear) core-target interactions give rise to complex reactions, which appear as a broad distribution at lower energies.

Fig. 3
Proton pick-up reactions of the ^{11}Be projectile on a beryllium target,. The intensity of the resulting isotopes of boron is shown as a function of the particle-identification signal, a combination of the signals from ΔE_2 and E_3 from the detector telescope, see Fig. 1. The total cross-section for all particle stable boron isotopes is 35±4 mb, so the single-proton pick-up leading to ^{12}B has a cross-section of about 5 mb.

Fig. 4
The "wounded halo" seen in its rest system after the collision with the target nucleus moving away to the right. The target has not touched the core of the halo system. The missing part of the wave function is denoted $\delta\psi_0$ in the text. The diagram below shows the coordinate system and the planar cut-off approximation. The swift passage of the target takes place in the direction of the z-axis (perpendicular to the plane of the paper) and the impact parameter b is on the x axis. The final state is one in which the charged (^{10}Be) core recoils along the negative x axis and at the same time the halo has a cylindrical wound. Following Glauber [21] we approximate in the present paper the wound by a planar cut-off at b_l.

Fig.5
Angular distribution from the gold target of fast neutrons ($26<E_n<80$ MeV) in coincidence with a ^{10}Be fragment detected in the counter telescope. The estimate based on Coulomb-excitation theory is shown as short dashes (here marked CE, in

our previous paper [23] called ZR). The full-drawn estimate (marked SUD) includes Coulomb *and* diffraction dissociation in the sudden approximation with a planar cut-off such as outlined in Section 3.4. In the absence of the Coulomb force the same calculation would lead to the curve marked SDIF. The curve with long dashes marked 1*s* is the intrinsic momentum distribution of the halo transformed, as were the other calculations, to an angular distribution in laboratory coordinates. This curve is normalized to go through the points near zero degrees, while the others are on an absolute scale with no free parameters.

Fig. 6
As Fig. 5 but for titanium and beryllium targets. The full-drawn curves are calculations including Coulomb and diffraction dissociation in the sudden approximation with a planar cut-off. The dashed curve (marked SCYL) represents diffraction dissociation on the Be target in the sudden approximation with a cylindrical "wound"; this was the estimate shown in [23]. Note that taking the target size explicitly into account improves the agreement with the measured shape; the effect on the integral cross-section is small, see the footnote to Table 1.

Fig. 7
The experimental points show the double-differential neutron cross-section for the gold target and calculated from the time-of-flight information recorded with the one detector placed at 0^0 and two at 1.48^0. The full-drawn curve represents a calculation that averages over the three detectors and over the beam energy, which varies from 44.1 to 36.9 MeV/u through the target. (The energy-loss calculations were based on Hubert et al. [27]). The dashed curves are calculations for a thin target and for the mean energy of 40.5 MeV, long dashes for 0^0 and short ones for 1.48^0.

Fig. 8
As Fig. 7 but for six detectors placed with two each at the angles 2.44, 3.39 and 4.40 degrees. The full-drawn curve is again a double average over angle and beam energy and the dashed curve the thin-target prediction for the angle 3.39^0 and a beam energy of 40.5 MeV.

Fig. 9
The experimental dissociation cross-sections for the reaction (^{11}Be,^{10}Be+X). The full-drawn lines are the calculated contributions from absorption, inelastic reactions (i.e. final states of ^{11}Be consisting of ^{10}Be and a free neutron) and (top) the sum of the two. The dashed line has been calculated with the nuclear terms set equal to zero. It shows what Coulomb dissociation alone would give in the same calculation. The inelastic nuclear contribution in the absence of Coulomb terms can be obtained by setting Z_2=0. The result would be indistinguishable from the absorption contribution and is not shown.

Fig. 10
Angular distributions of fast neutrons ($25<E_n<75$ MeV) produced by a 41 MeV/u beam of Be on a target of beryllium. The filled circles are the restricted inclusive events, i.e. events not accompanied by an outgoing ^{10}Be. Also shown are two sub-

sets of exclusive events corresponding to coincidences with outgoing helium (Z=2, filled triangles) and lithium (Z=3, open squares) ions, independent of their mass. The curve, arbitrarily normalized to fit the points at zero degrees, is the angular distribution obtained by transforming to laboratory coordinates the momentum distribution of a finite-size square well with depth adjusted to reproduce the experimental neutron separation energy of 0.5 MeV. The integrated restricted inclusive cross-section is 1.5±0.3 barn.

Fig.11
Same as Fig.10, but for a titanium target. The integrated restricted inclusive cross-section is 1.6±0.3 barn and that for the gold target (not shown) is 1.0±0.4 barn.

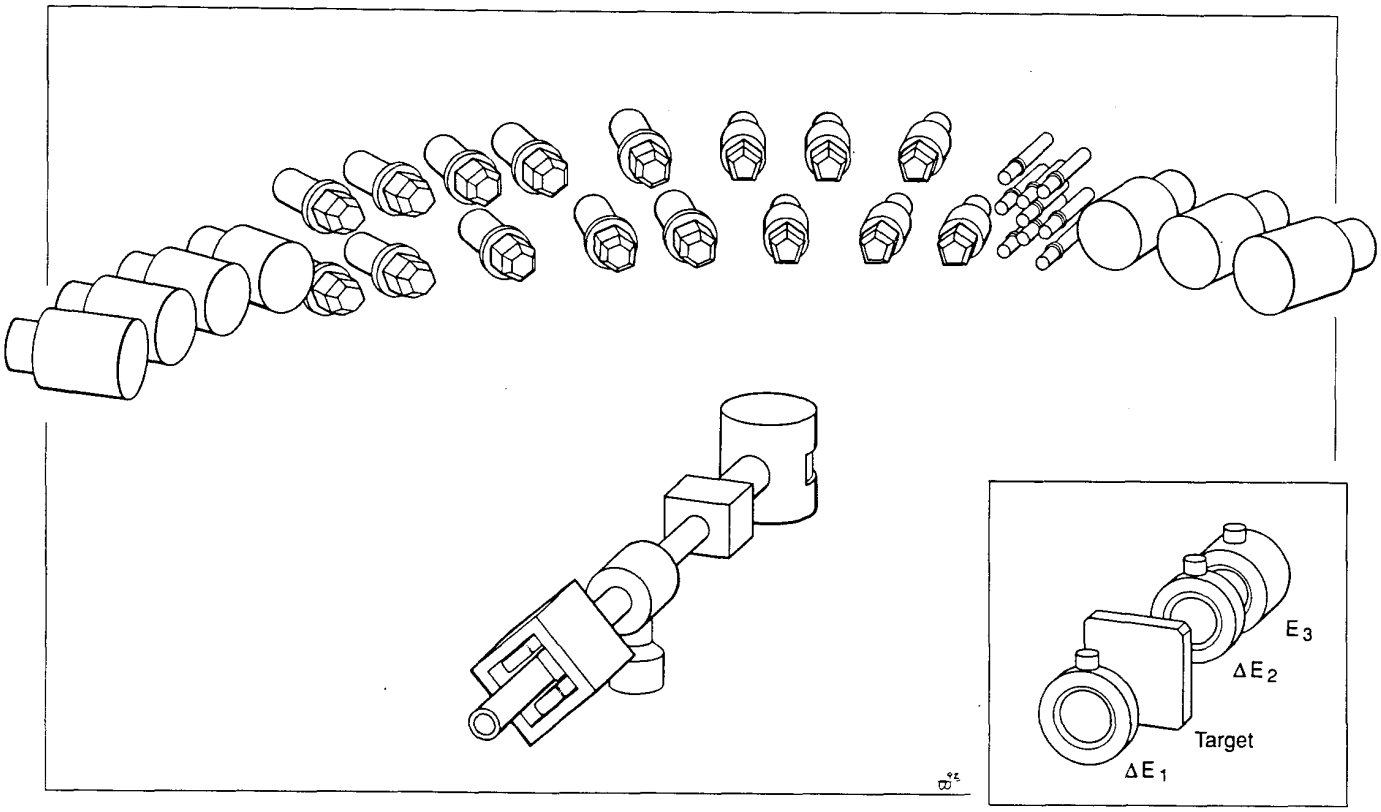

R. Anne et al., Exclusive and Restricted Inclusive.... Fig. 1

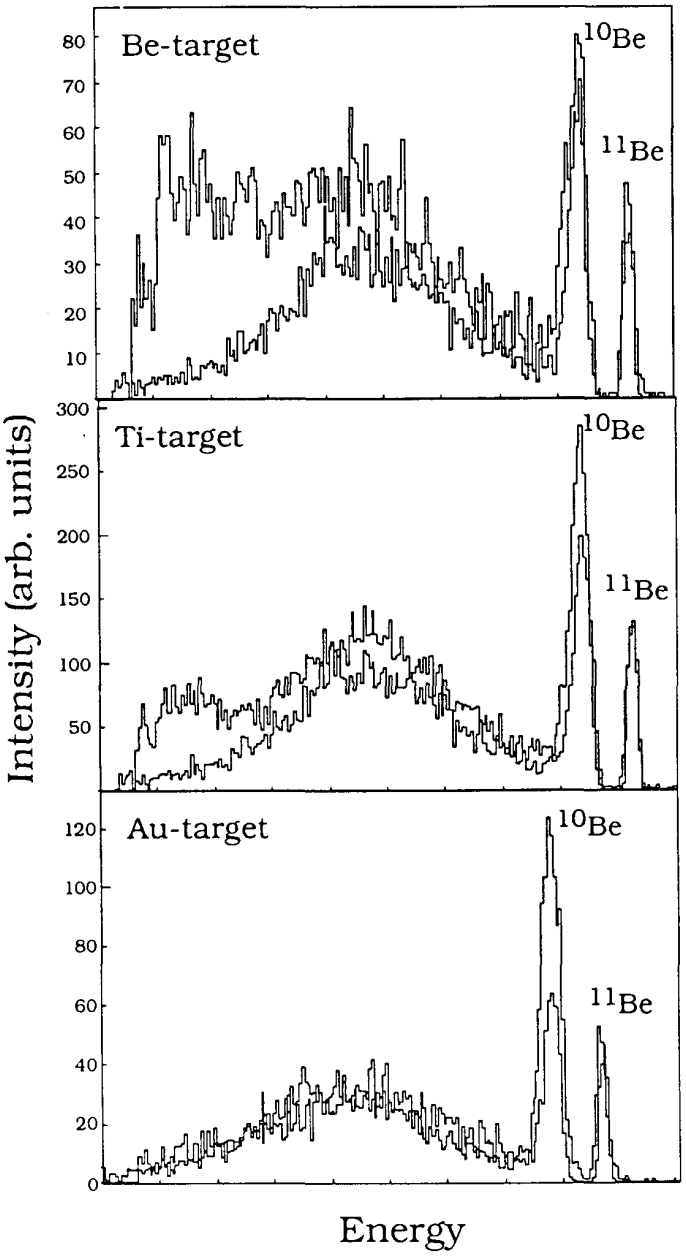

R. Anne et al., Exclusive and Restricted Inclusive....

Fig. 2

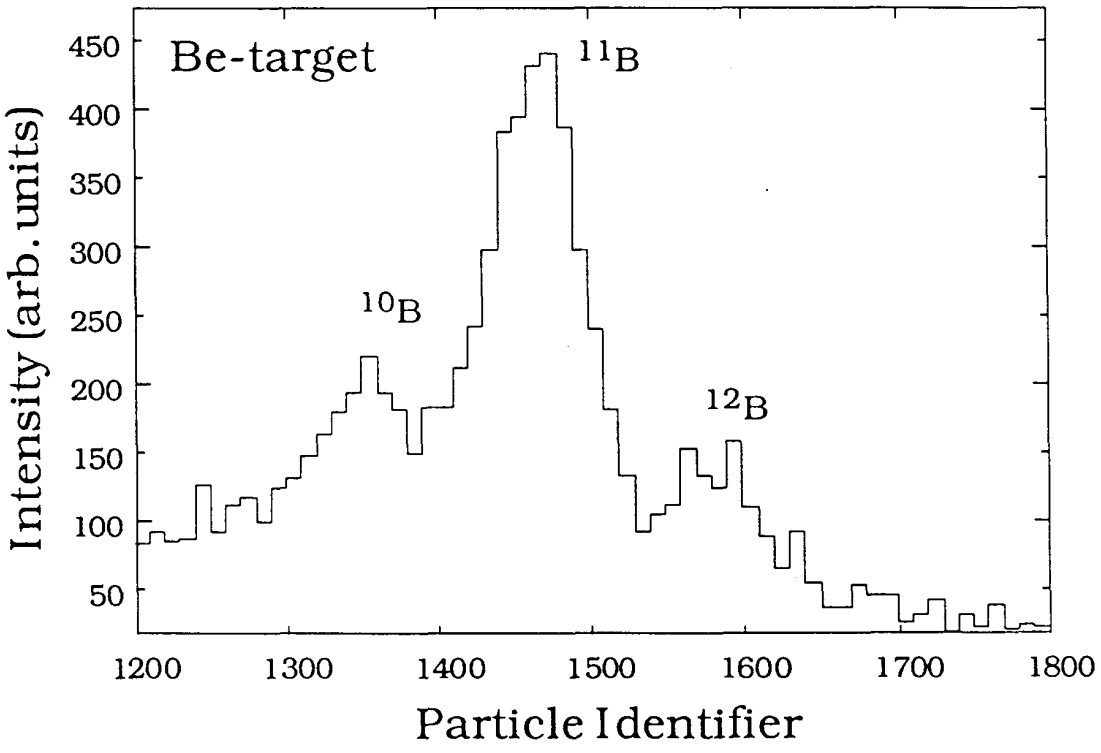

R. Anne et al., Exclusive and Restricted Inclusive....

Fig. 3

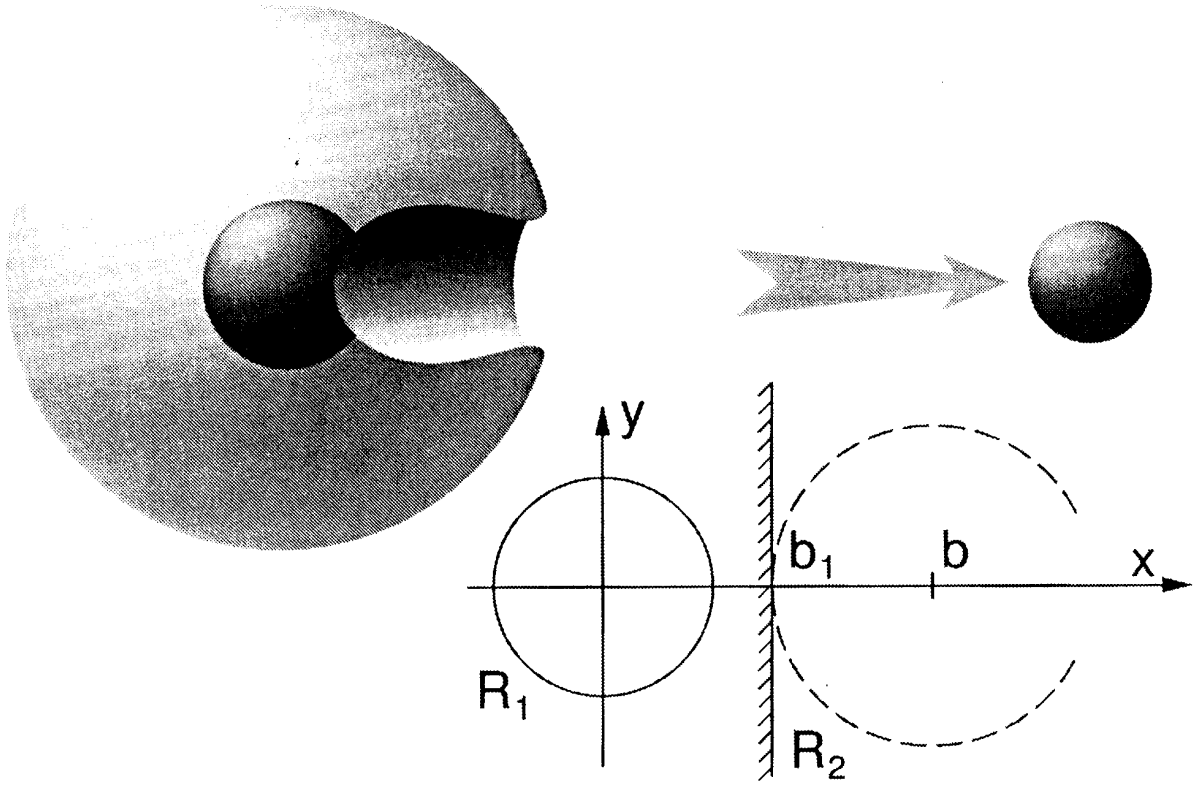

R. Anne et al., Exclusive and Restricted Inclusive....

Fig. 4

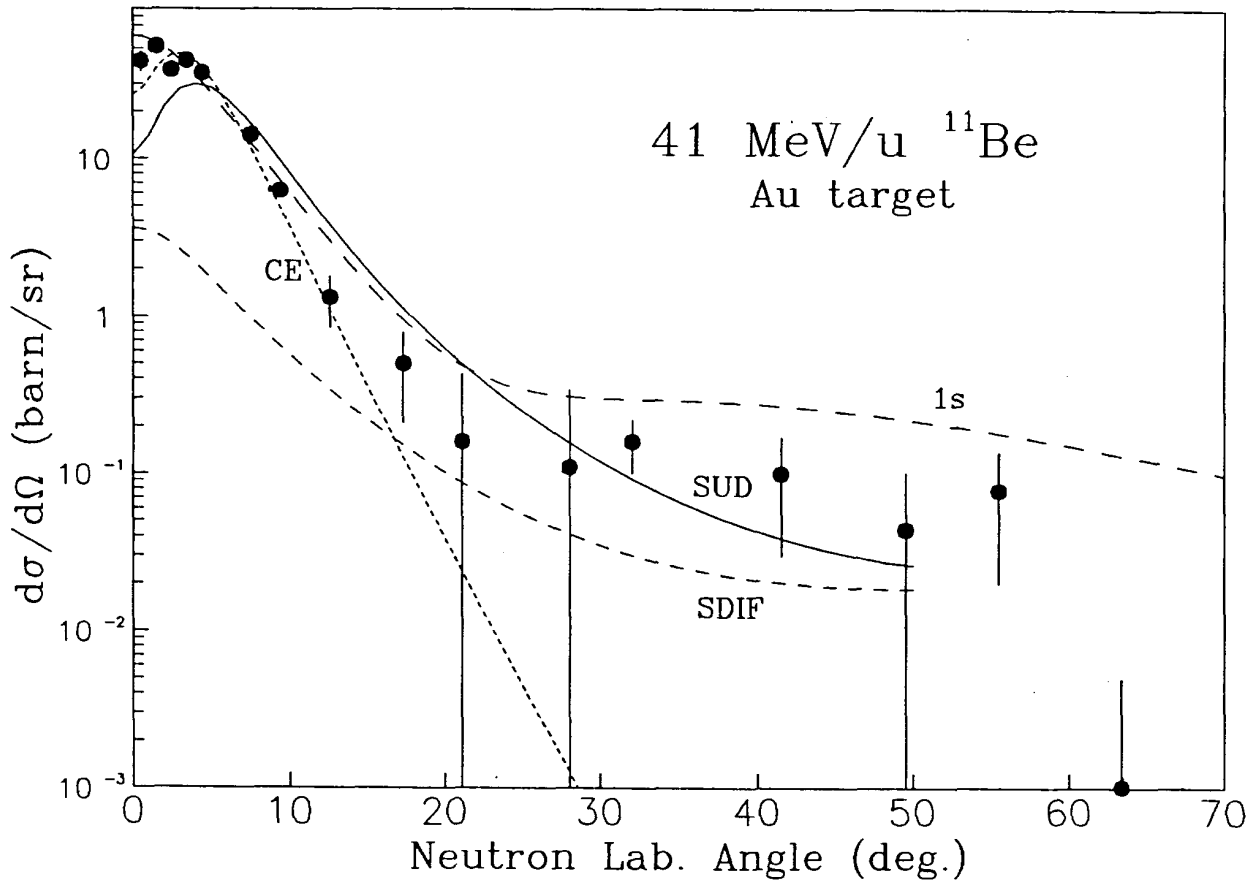

R. Anne et al., Exclusive and Restricted Inclusive.... Fig. 5

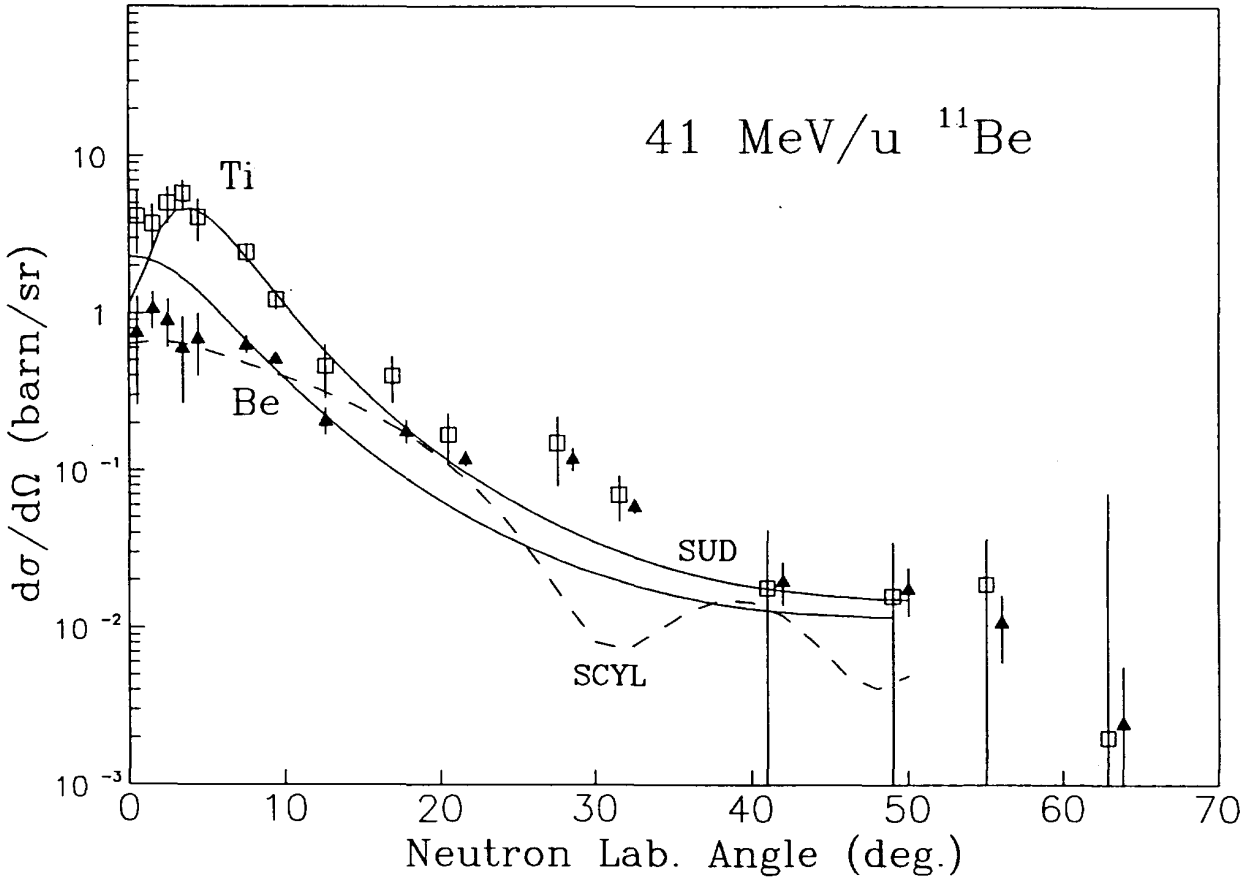

R. Anne et al., Exclusive and Restricted Inclusive.... Fig. 6

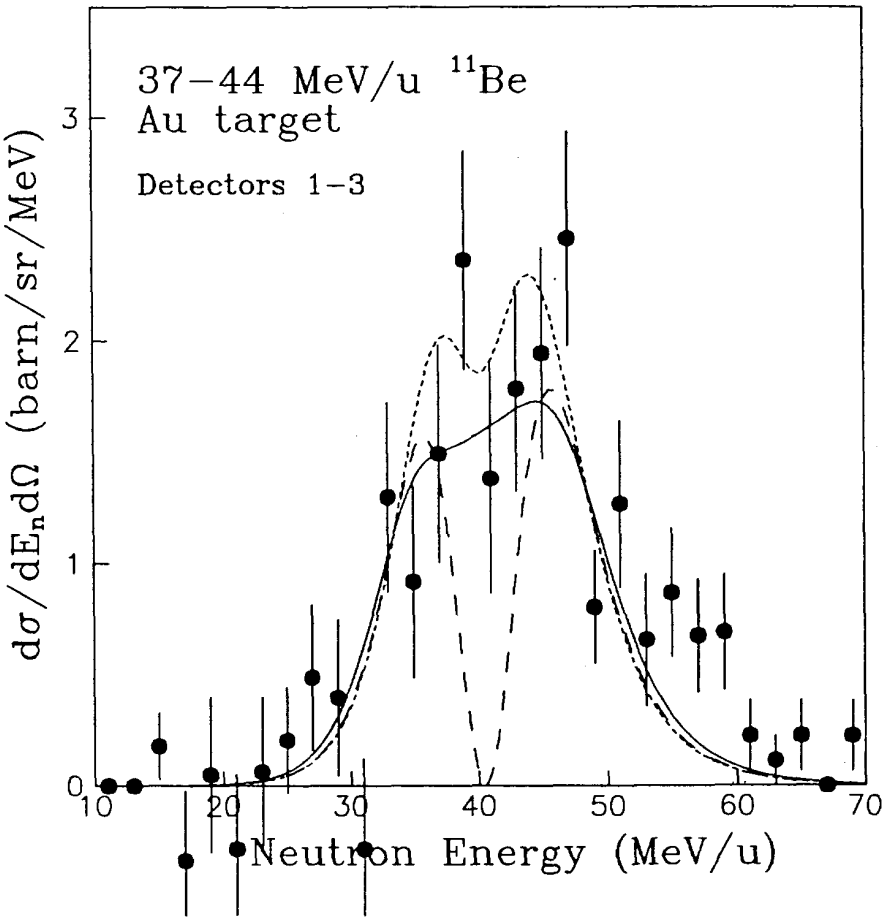

R. Anne et al., Exclusive and Restricted Inclusive.... Fig. 7

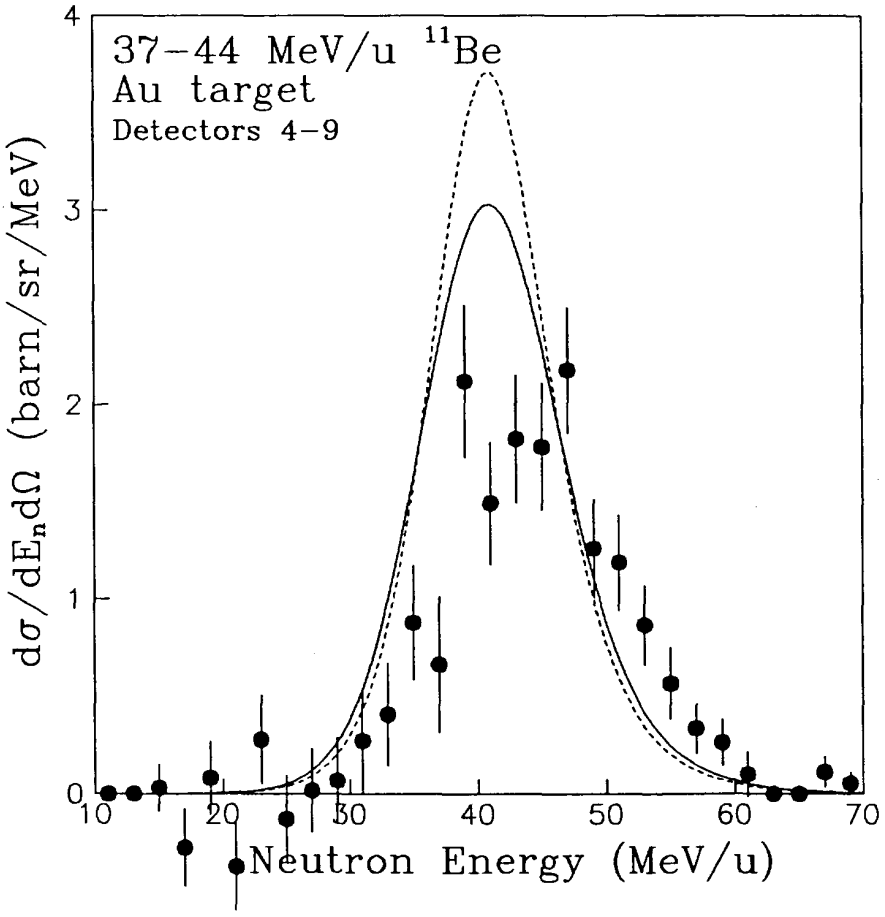

R. Anne et al., Exclusive and Restricted Inclusive....

Fig. 8

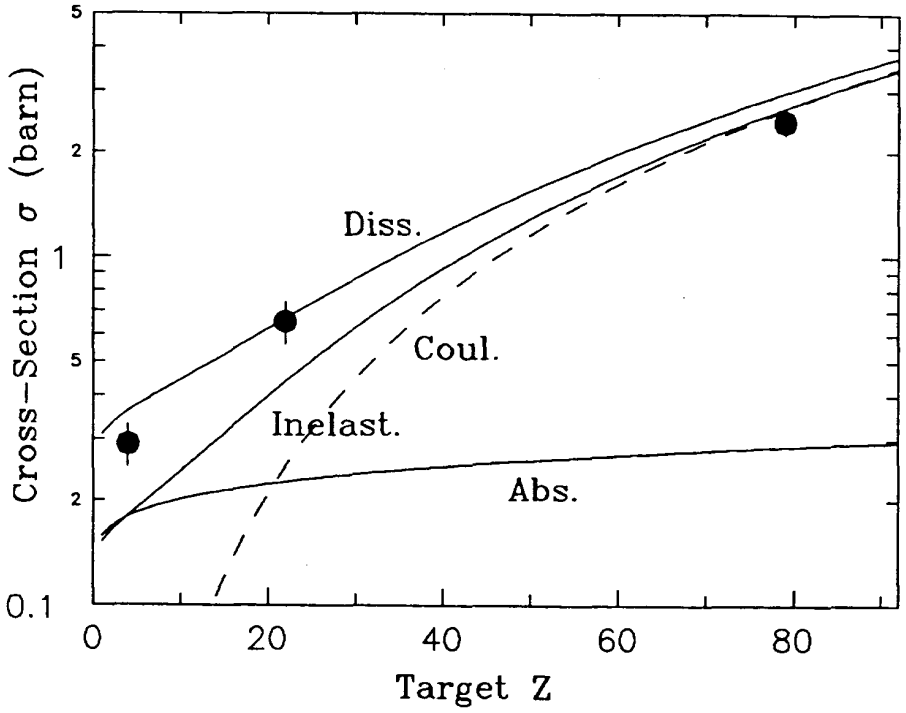

R. Anne et al., Exclusive and Restricted Inclusive.... Fig. 9

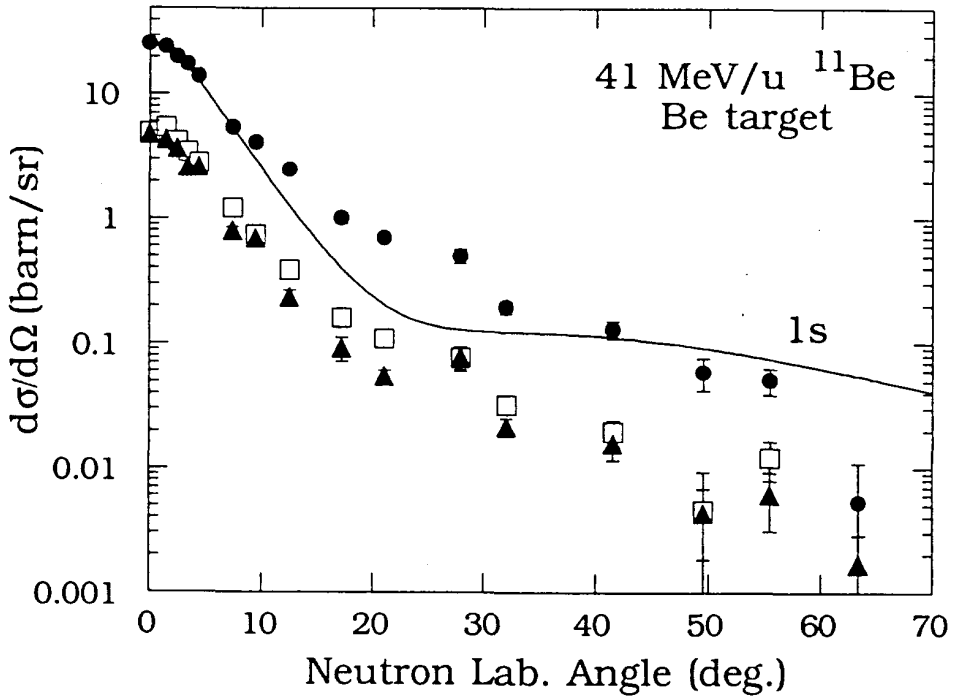

R. Anne et al., Exclusive and Restricted Inclusive....

Fig. 10

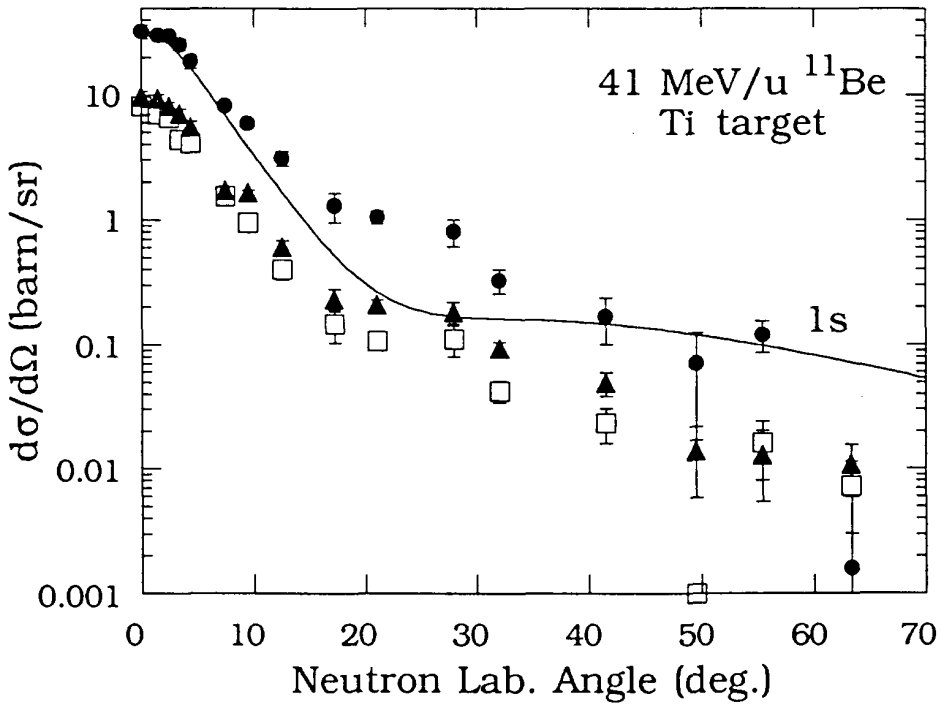

R. Anne et al., Exclusive and Restricted Inclusive.... Fig. 11